

Yajuan Ji¹

National Key Laboratory of Science and
Technology on Helicopter Transmission,
Nanjing University of Aeronautics & Astronautics,
Nanjing 210016, China
e-mail: jiyajuan@foxmail.com

Qingwen Dai^{1,2}

National Key Laboratory of Science and
Technology on Helicopter Transmission,
Nanjing University of Aeronautics & Astronautics,
Nanjing 210016, China
e-mail: daiqingwen@nuaa.edu.cn

Wei Huang

National Key Laboratory of Science and
Technology on Helicopter Transmission,
Nanjing University of Aeronautics & Astronautics,
Nanjing 210016, China
e-mail: huangwei@nuaa.edu.cn

Xiaolei Wang

National Key Laboratory of Science and
Technology on Helicopter Transmission,
Nanjing University of Aeronautics & Astronautics,
Nanjing 210016, China
e-mail: xlwanggo163@163.com

On the Thermocapillary Migration at the Liquid and Solid Aspects

Thermocapillary migration is an interfacial phenomenon that describes liquid flow on a nonisothermal surface from warm to cold regions in the absence of external forces. It is a typical lubricant loss mechanism in tribosystems. To ensure continued reliability of lubricated assemblies, knowledge of the migration capacity of different liquids and solids is needed. In the present work, migration experiments were conducted on various liquid lubricants on different solid surfaces. It was found that polar lubricants such as ionic liquids and polyethylene glycol hardly migrate on the tested surfaces, and the antimigration capacity of the polytetrafluoroethylene surface was discovered to be very high. Particular attention is paid to the migration mechanism associated with surface tension and contact angle. General guidelines for evaluating the migration capacities of different liquids on solids are proposed. [DOI: 10.1115/1.4043972]

Keywords: thermocapillary migration, polar lubricant, surface tension, contact angle

1 Introduction

In tribosystems, liquid lubricants are often employed to decrease friction and wear rate between rubbing surfaces [1]. Typically, a process involving friction is always accompanied by energy dissipation, which generates heat and results in an uneven distribution of temperature on the surface [2]. A liquid lubricant placed on a nonisothermal rubbing surface will migrate toward colder portions of the surface in the absence of external forces. This is because a thermal gradient alters the surface tension of a liquid and generates a shear force on the free surface, thus contributing to the propulsion [3–8].

Such thermal flow is crucial in industrial applications, such as miniature rolling bearings, hard disks, and microfluidics [9–11]. In some situations, liquid migration is beneficial as it promotes lubricant wetting on the rubbing surface [12]. In others, one may desire to limit liquid migration to ensure adequate lubrication at the contact area [13]. Moreover, special attention should be paid to liquid migration in space machinery as they work in an extremely wide temperature range (–150 to 150 °C), owing to which liquid lubricants can run away easily under a thermal gradient [14]. Note that because lubricants in space machinery are always present in limited quantities and cannot be refueled, it is vital to regulate and control their migration to guarantee a long lifetime and stable running of the machinery [15].

Thermocapillary migration is a natural phenomenon occurring at the liquid–solid interface, and a large number of studies have been conducted on the behavior of these phases in the past. From the liquid aspect, modifying the properties of liquid lubricants, such as increasing their viscosity [16], enhancing the cohesiveness of lubricant molecules [17], or using ferrofluids as lubricants subjected to an external magnetic field [18], has been proven to be effective

ways to obstruct migration. From the solid aspect, roughening the surface [19], fabricating isotropic structures [20], and using topography gradients [21] or wettability gradients [22] are feasible methods to regulate liquid migration.

Such studies promoted a significant progress in migration research, and some of these techniques have been successfully applied in space [23]. However, in industrial application, a great number of solid materials and liquid lubricants are employed depending on the working conditions. Without a comprehensive understanding of the migration performances of different lubricants on different surfaces, it would be rather difficult to design suitable and effective antimigration strategies. A review of the available literature indicates that this knowledge is currently lacking.

Hence, in this investigation, five typical liquid lubricants and four solid materials were chosen and the migration experiments were conducted correspondingly. Particular attention was paid to the migration mechanism associated with surface tension and contact angle. Based on the results, general guidelines for evaluating the migration capacities of different liquids and solids are proposed.

2 Experiment

2.1 Liquids. Two major liquid lubricant categories, nonpolar and polar, were used in this study, as shown in Table 1. Generally, the kinematic viscosities of these lubricants are of the same order of magnitude. In the case of nonpolar lubricants, three subcategories,

Table 1 General information of the lubricants used in this study

Category	Lubricants	Molecular formula	Kinematic viscosity (mPa · s) (at 40 °C)
Nonpolar oil	PAO	$C_{10}H_{21}(C_{10}H_{20})_nH$	16.6
	Paraffin oil	$n-C_nH_{2n+2}$ ($n = 16–20$)	26.9
	Diester	$C_{26}H_{50}O_4$	21.2
Polar oil	PEG	$H(OCH_2CH_2)_nOH$	22.5
	IL	$C_8H_{11}O_4N_3S_2F_6$	32.1

¹The authors contributed equally to the work.

²Corresponding author.

Contributed by the Tribology Division of ASME for publication in the JOURNAL OF TRIBOLOGY. Manuscript received December 28, 2018; final manuscript received June 5, 2019; published online June 27, 2019. Assoc. Editor: Noel Brunetiere.

ambient atmosphere due to its very low chemical reactivity [27]. Si is widely used in micro and nano devices in space. Therefore, these four materials were chosen for migration tests.

First, test specimens ($76 \times 30 \times 3$ mm) were fabricated from stainless steel (SUS 316) and the testing surfaces were polished to a final surface roughness (R_a) of $0.02 \mu\text{m}$ together with a high degree of flatness. Later, Au, Ti, and PTFE coatings were fabricated on these steel surfaces via physical vapor deposition, electrodeposition, and spray-painting techniques, respectively. Figure 3 shows the components of the prepared Au, Ti, and PTFE coatings, as well as their surface morphology and roughness. Surface roughness (S_a) is measured at three different positions on each surface; the average S_a values of Au, Ti, and PTFE coatings were approximately 8, 30, and 1020 nm , respectively. As the Si specimen was directly processed from a silicon wafer, its S_a was approximately 3 nm (morphology not shown).

2.3 Experimental Setup. Figure 4 shows the experimental apparatus designed for this study. The substrate was tightly attached to heating and cooling elements, on which all the migration tests were performed. The available length for migration tests was 50 mm, and by setting the heating and cooling elements to 0°C and 110°C , respectively, a thermal gradient of $2.2^\circ\text{C}/\text{mm}$ was

generated on the surface. Thermography results confirmed a uniform thermal gradient, and it is accurately calibrated using thermocouples. Generally, a high thermal gradient yields a faster migration velocity (limited by the available length for migration) while a low thermal gradient results in a longer testing time. Therefore, a thermal gradient of $2.2^\circ\text{C}/\text{mm}$ was used for the sake of comparison.

Prior to each migration test, specimens were ultrasonically cleaned with acetone and alcohol, rinsed with deionized water, and blow-dried with nitrogen. A droplet of a certain volume was placed on the warm side after the formation of a thermal gradient, and the dynamic migration process was monitored by a digital camera. From the front edge of the droplet observed in the extracted frames, the migration distance and average velocity were calculated.

3 Results

Figure 5(a) shows the typical migration process of a $5 \mu\text{L}$ diester droplet on Au, Ti, Si, and PTFE surfaces. As expected, under a thermal gradient of $2.2^\circ\text{C}/\text{mm}$, droplets migrate from warm to cold regions. Migration occurs to varying extents on different surfaces while droplets remain stationary on the PTFE surface during the entire test time. Figure 5(b) illustrates the relationship between migration distance and average migration velocity over 30 s. It can

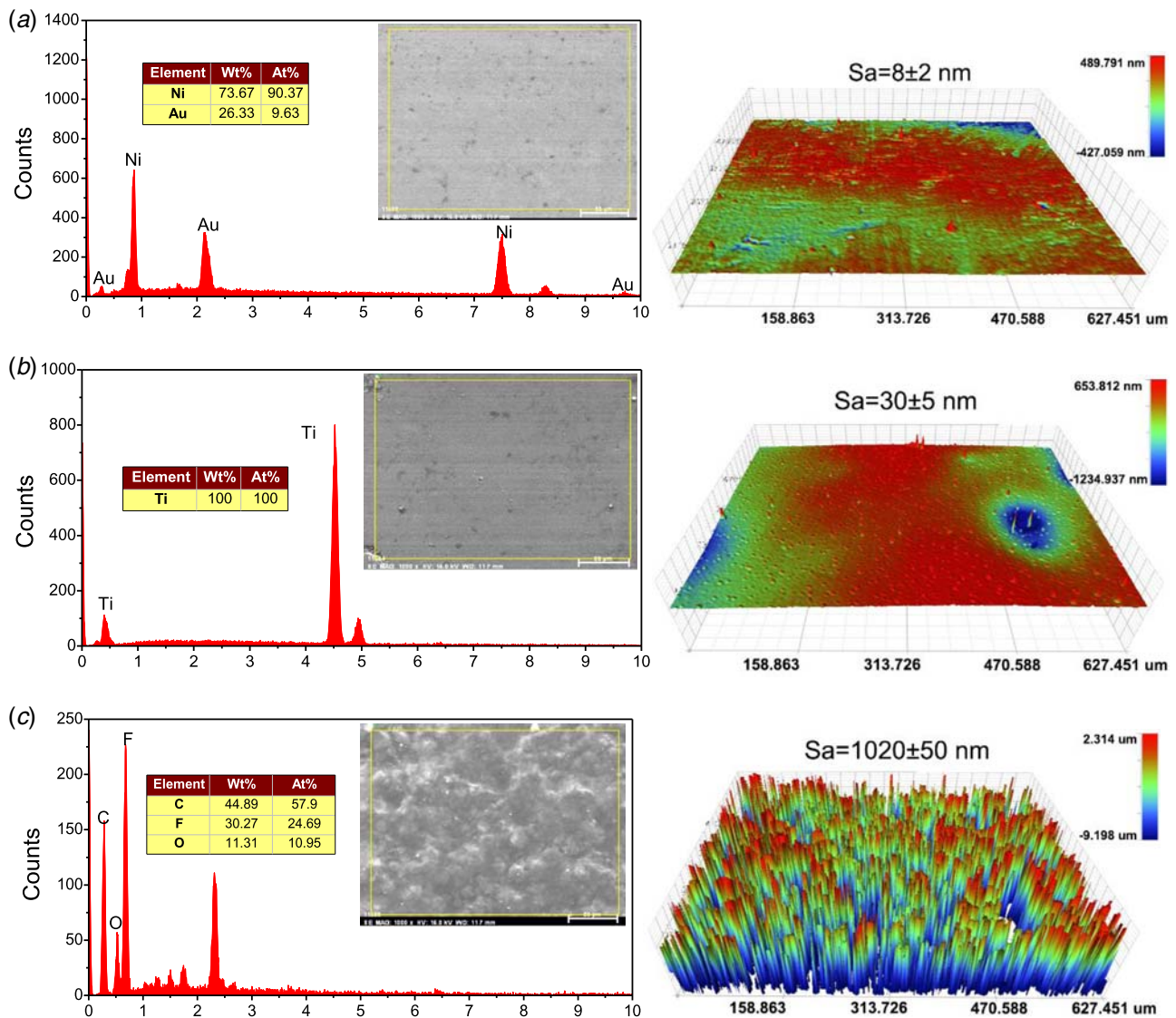


Fig. 3 Surface morphology and roughness of (a) Au, (b) Ti, and (c) PTFE coatings

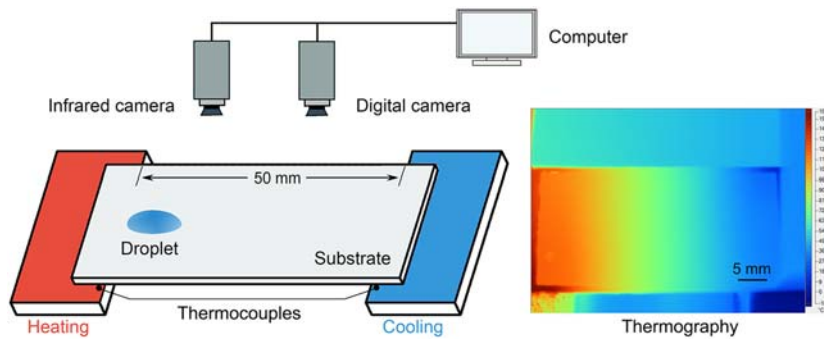


Fig. 4 Schematic illustration of the apparatus used in this study

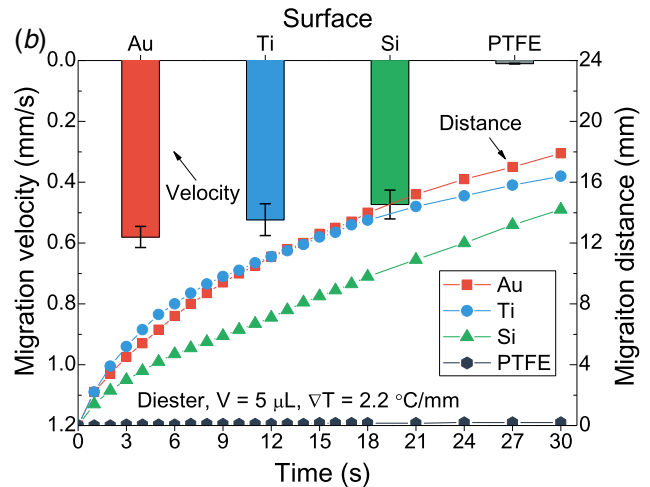
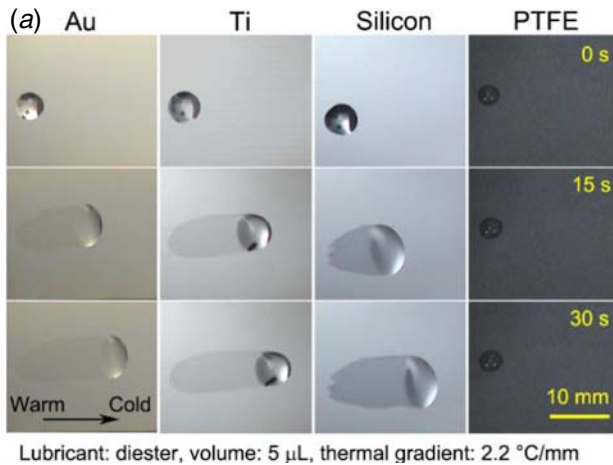


Fig. 5 Migration of diester droplets on different surfaces: (a) the migration phenomenon and (b) migration distance and average migration velocity over 30 s

be seen that the initial migration distance increased rapidly and after 15 s, this increase became linear. Referring to the migration distance curve, 30 s is enough to distinguish the differences among the migration capacities of different liquids on different solids. Therefore, the average migration velocities over 30 s is employed in Secs. 3 and 4. Droplets on the Au surface exhibited a high migration velocity of ~ 0.6 mm/s. Meanwhile, droplet velocities were ~ 0.52 mm/s on the Ti surface and ~ 0.45 mm/s on the Si surface. However, on the PTFE surface, the migration velocity was nearly zero.

Figure 6 presents the migration processes and velocities of PAO, diester, paraffin oil, PEG, and IL droplets ($5 \mu\text{L}$) on an Au surface under a thermal gradient of $2.2 \text{ }^\circ\text{C}/\text{mm}$. Obvious differences exist in the migration performance of different lubricants on the same surface. The migration velocity of PAO is the highest, and it is interesting to note that polar lubricants (PEG and IL) hardly migrated on the Au surface.

To confirm the experimental results shown in Figs. 5 and 6, a comprehensive investigation was conducted on the migration capacities of all the tested lubricants on different surfaces. As shown in Fig. 7(a), migration velocities of $5 \mu\text{L}$ droplets follow the order of $\text{PTFE} < \text{Si} < \text{Au} < \text{Ti}$; none of the tested lubricants could migrate on the PTFE surface. The velocities of PEG and IL droplets on all the tested surfaces were nearly zero while the migration velocities of nonpolar liquids followed the order of $\text{paraffin oil} < \text{diester} < \text{PAO}$ on all the tested surfaces.

Referring to Figs. 5 and 6, it is interesting to note that the surface area of migrating droplets changes as the migration progresses, except in the case of PEG and IL droplets (because they remain stationary all the time). By extracting key frames from the recorded video, the relationship between surface area and elapsed time is obtained and shown in Fig. 7(b). In the case of paraffin oil, diester,

and PAO droplets, their surface areas were initially similar and increased rapidly in the first few seconds; as time elapsed, their surface area gradually became constant. It is noticed that the magnitudes of surface areas follow the order of $\text{paraffin oil} > \text{diester} > \text{PAO}$, which is opposite to the trend of migration velocity shown in Fig. 7(a).

Even after increasing the droplet dosage to $10 \mu\text{L}$, as shown in Fig. 8, PTFE surfaces and PEG and IL liquids still exhibited

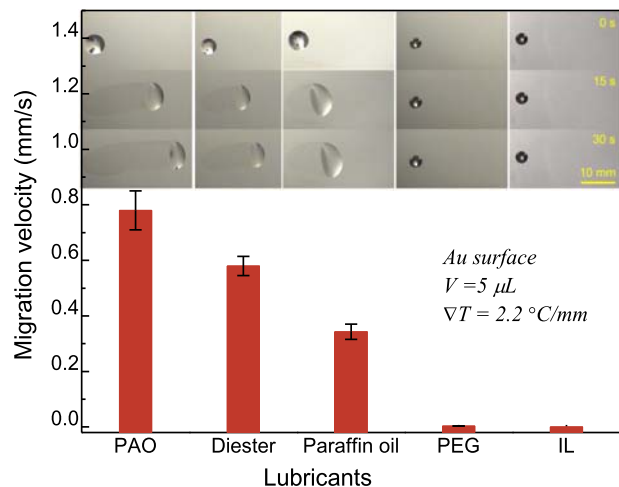


Fig. 6 Migration processes and velocities of different lubricants on Au surfaces

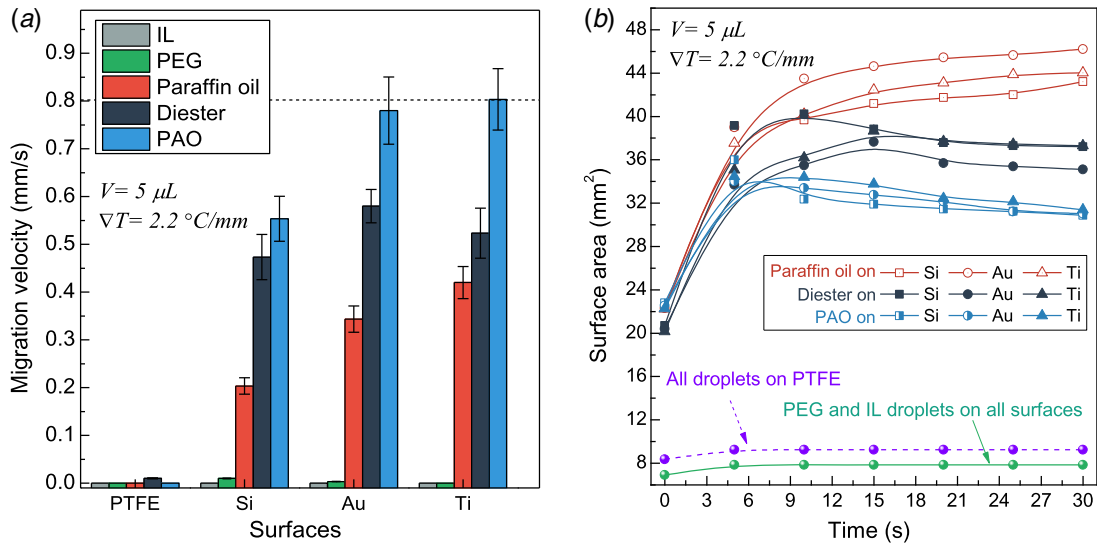


Fig. 7 (a) Comparison of the migration capacities of all the tested lubricants (5 μL droplets) on different surfaces and (b) variation in the surface area of migrating droplets

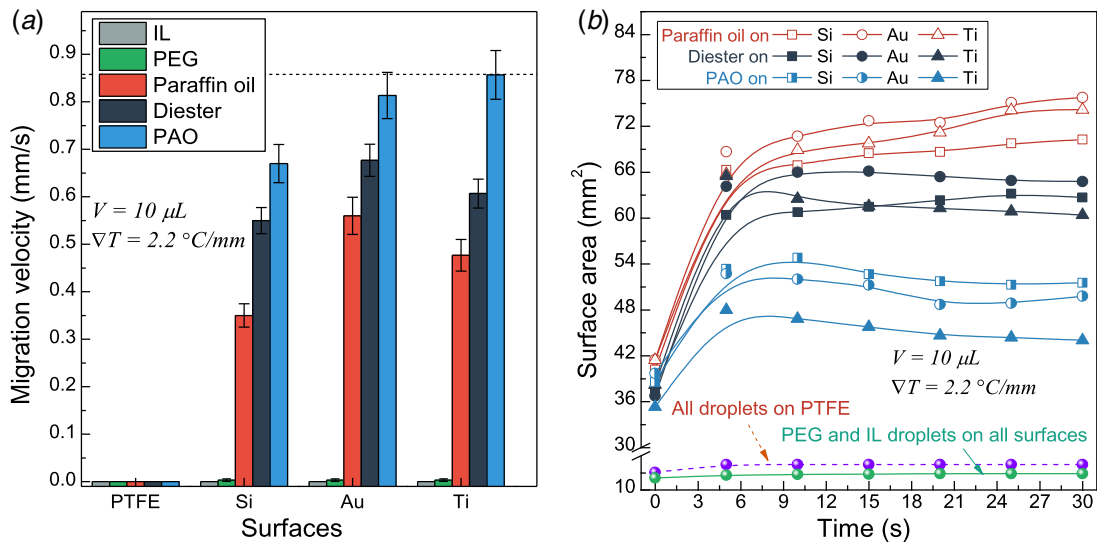


Fig. 8 (a) Comparison of the migration capacities of all the tested lubricants (10 μL droplets) on different surfaces and (b) variation in the surface areas of migrating droplets

excellent antimigration capacities. Meanwhile, the migration velocities of liquid lubricants followed the order PEG or IL < paraffin oil < diester < PAO on all other tested solid surfaces. Surface areas of the migrating droplets decreased in the order of paraffin oil, diester, PAO, and PEG or IL. Similar to the results shown in Fig. 7, the general trends of variation corresponding to migration velocity and surface area are consistent, except for an increase in their amplitude.

4 Discussion

4.1 Migration Mechanism. From the experimental results, it is inferred that thermocapillary migration is directly correlated to the properties of solids and liquids. Theoretically, Brochard's reports [28], Ford's and Nadim's investigations [29], and our previous studies [30] prove that droplets with small contact angles can be regarded as thin films with curved rims. In the case of the migrating liquid droplets considered in the present work, their contact angles are relatively small (<16 deg), and hence, the variable component of the droplet film at the rim is much smaller than the constant

component. Therefore, we consider a simple geometrical model to analyze the migration process, as shown in Fig. 9. When a liquid droplet is placed on a nonisothermal surface, interfacial tensions on the warm and cold sides are unbalanced, which exerts a driving force for migration. This driving force (per unit length along the x direction) can be written as F_T

$$F_T = (\gamma \cos \theta)_F - (\gamma \cos \theta)_B \quad (2)$$

where γ and θ represent the liquid–gas interfacial tension and contact angle, respectively, and subscripts F and B represent the front and back positions, respectively.

The thermal gradient (C_T) is constant on the solid surface, i.e., $C_T = \partial T / \partial x = \text{const}$, when it is assumed that temperature field within the droplet is exactly the same as that of the solid. Combining this with Eq. (1), the relationship between interfacial tensions at back and front positions along the droplet can be described as

$$\gamma_F = \gamma_B + C_T \gamma_T L \quad (3)$$

where L is the width of the droplet.

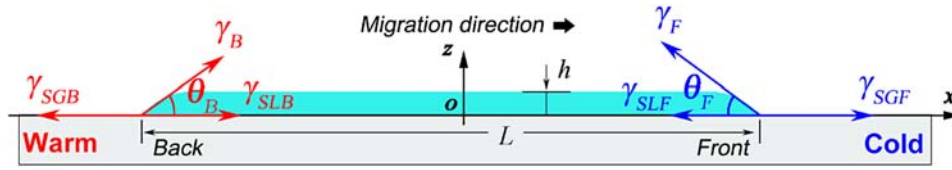


Fig. 9 Cross section of a migrating liquid droplet on a nonisothermal surface

Substituting Eq. (3) into Eq. (2), the driving force can be expressed as

$$F_T = C_T \gamma_T L \cos \theta \quad (4)$$

As migration progresses, the advancing edge of the droplet wets forward, while the receding edge dewets. This wetting and dewetting process inevitably involves contact angle hysteresis at the rim. Although Cheng et al. [31] and several other researchers [32,33] proposed a complicated theoretical model to predict the motion after taking hysteresis into account, differences between the migration capacities of different liquids on different solids are still unclear. In fact, the contact angle hysteresis effect yields a lateral retention force (F_L) at the rim, generating a resistance to motion. This force can be described as [34,35]

$$F_L = \gamma (\cos \theta_A - \cos \theta_R) \quad (5)$$

where θ_A and θ_R are the advancing and receding contact angles, respectively.

It can be inferred that the thermal driving force (F_T) originating from interfacial tension gradients must overcome the lateral retention force (F_L) before the droplet can migrate, i.e., $F_T - F_L \geq 0$. Hence, a dimensionless number can be employed to check whether migration will occur or not

$$H^* = \frac{F_T - F_L}{\gamma} = \frac{C_T \gamma_T L \cos \theta}{\gamma} - (\cos \theta_A - \cos \theta_R) \quad (6)$$

By substituting the measured surface tensions (Fig. 2) and contact angles (Table 2) into Eq. (6), the values of H^* for all the lubricants tested on different surfaces were calculated, as shown in Fig. 10. It can be seen that for nonpolar lubricants (PAO, paraffin oil, and diester), the values of H^* were positive on Au, Ti, and Si surfaces and negative on the PTFE surface. In the case of polar PEG and IL, the values of H^* were negative on all the tested surfaces. Referring to the experimental results shown in Figs. 7 and 8, it can be noted that a positive H^* results in migration while a negative H^* will not. Therefore, estimating the value of H^* provides preliminary information on the migration capacity of a liquid droplet on a solid surface.

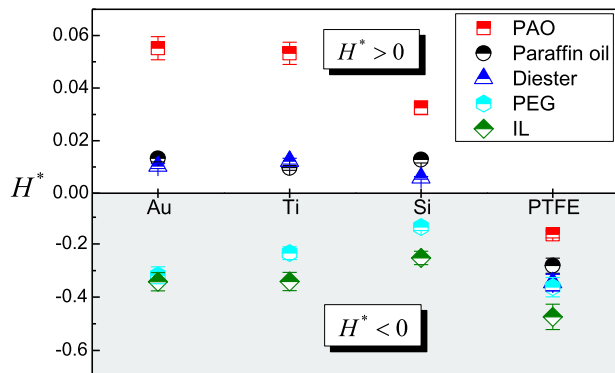


Fig. 10 Calculated values of the dimensionless number (H^*) for all lubricants on different surfaces

4.2 Nonpolar Lubricants. Considering the fact that the dimensionless number H^* represents the magnitude of the driving force, it is asserted that a larger H^* yield a faster migration velocity. In the case of nonpolar lubricants, the H^* value of PAO was the largest and, therefore, its migration velocity was the highest as shown in Figs. 7 and 8. However, obvious differences exist between the migration velocities of paraffin oil and diester even though their H^* values are nearly the same; hence, there should be other reasons to explain this discrepancy.

Previous studies [36,37] suggested that after ignoring gravitational and capillary forces, a simple mathematical expression can be used to calculate the migration velocity (U) of a droplet on an ideally smooth surface, $U \approx C_T \gamma_T h / 2\mu$, where h and μ denote the thickness and dynamic viscosity of the droplet, respectively. In the present study, the investigated lubricants exhibit changeable cross-sectional morphologies depending on the solid surface used and there is a trail of oil left behind by the migrating droplet (Figs. 5 and 6), which makes it difficult to directly calculate the theoretical migration velocity without using the value of h . Nevertheless, the variation tendency of the surface area of migrating droplets reflects changes occurring in the thickness of the droplet. The previously-stated equation indicates that migration velocity is inversely proportional to the surface area and dynamic viscosity μ of a liquid. The dynamic viscosity (Table 1) and surface area (Figs. 7 and 8) of paraffin oil droplets are higher than those of diester, which is why the migration velocity of the former is lower when compared to the latter.

4.3 Polar Lubricants. In the case of polar lubricants, their H^* values were negative; as the chemical structures in Fig. 2 show, the major difference between polar and nonpolar lubricants is the presence of polar groups in polar lubricant molecules. Generally, these molecules can adsorb onto metal surfaces, forming an adsorption layer at the liquid/solid interface, and contribute to the adhesion force between the liquid and the solid [38]. Moreover, when studied at the molecular level, it is found that this layer is indeed composed of ions, which are in direct contact with the substrate. It can be confirmed that the orientation and position of these ions are well ordered at the interface while metals are polarizable with free electrons [39]. When a polar liquid is placed on a metal solid surface, a powerful Coulombic force is generated between the layer and free electrons, which increases bonding strength between the liquid and the substrate, resulting in a strong adsorption energy at the interface [40]. The contact line at the front edge of a polar liquid is pinned and significant contact angle hysteresis is involved. Consequently, the thermal driving force is insufficient to overcome the lateral resistance force.

4.4 Solids. Most solids are naturally rough and chemically heterogeneous; these characteristics are associated with the pinning of contact lines on surface defects, which weakens the spreading capacity of a liquid on a solid. This weakening effect significantly influences migration when surface roughness is of a considerable magnitude. Surface roughness of the PTFE surface considered in this study was approximately $1.02 \mu\text{m}$, which was much larger than that of Au, Ti, and Si surfaces; this is possibly one reason why liquid droplets hardly migrated on the PTFE surface. Note that the projected contact area of the droplets varies on Au, Ti,

and Si surfaces as migration progresses (Fig. 3(a)). This is because on a smooth surface, a liquid droplet tends to spread to the surrounding area and the thermal gradient contributes to forward migration. These effects together result in an elliptical droplet shape on Si ($Sa = 3$ nm) and Au ($Sa = 8$ nm) surfaces. Meanwhile, on the Ti ($Sa = 30$ nm) surface, numerous irregular microstructures are found (Fig. 3(b)) that hinder the droplet from spreading to the surrounding regions and resulting in a circular shape.

Contact angles reflect interactions between a liquid and a solid. The larger the contact angle between a solid and a liquid, weaker is the interaction between them. As the measured data in Table 2 show, contact angles between PTFE and all the tested lubricants are always very high. This means that interactions between the solid and liquid molecules are relatively weak, and hence, it is difficult for liquids to migrate on the PTFE surface. Meanwhile, on Si, Au, and Ti surfaces, the advancing, receding, and equilibrium contact angles of different lubricants are similar in magnitude and differences in their migration capacity originate mainly from the liquids tested.

5 Conclusions

Thermocapillary migration is an interfacial phenomenon of great importance in fundamental science and engineering applications. However, general knowledge on the migration mechanisms of different lubricants on different surfaces is currently lacking. Hence, experiments were conducted in this study to investigate the influence of the physical and chemical properties of solids (four material surfaces) and liquids (five lubricants) on thermocapillary migration. From the point of view of solids, a nonmetallic material with low surface tension, such as PTFE, hinders thermocapillary migration. Meanwhile, polar lubricants, such as polyethylene glycol and ionic liquids, exhibit a strong antimigration capacity. For potential industrial applications, especially in tribosystems, it is recommended to provide the contact angles of lubricants on solid surfaces or the surface tension coefficient of liquid lubricants. These parameters would help designers in evaluating the migration capacities of the tested surfaces and lubricants via the proposed dimensionless number.

Funding Data

- National Nature Science Foundation of China (Grant No. 51805252; Funder ID: 10.13039/501100001809).
- China Postdoctoral Science Foundation (Grant No. 2019M651822; Funder ID: 10.13039/501100002858).

References

- [1] Khonsari, M. M., and Booser, E. R., 2008, *Applied Tribology: Bearing Design and Lubrication*, John Wiley & Sons Ltd, Chichester.
- [2] Amiri, M., and Khonsari, M. M., 2010, "On the Thermodynamics of Friction and Wear—A Review," *Entropy*, **12**(5), pp. 1021–1049.
- [3] Tadmor, R., 2009, "Marangoni Flow Revisited," *J. Colloid Interface Sci.*, **332**(2), pp. 451–454.
- [4] Bormashenko, E., Bormashenko, Y., Gryniov, R., Aharoni, H., Whyman, G., and Binks, B. P., 2015, "Self-Propulsion of Liquid Marbles: Leidenfrost-Like Levitation Driven by Marangoni Flow," *J. Phys. Chem. C*, **119**(18), pp. 9910–9915.
- [5] Dai, Q., Khonsari, M. M., Shen, C., Huang, W., and Wang, X., 2017, "On the Migration of a Droplet on an Incline," *J. Colloid Interface Sci.*, **494**, pp. 8–14.
- [6] Dai, Q., Huang, W., Wang, X., and Khonsari, M. M., 2018, "Ringlike Migration of a Droplet Propelled by an Omnidirectional Thermal Gradient," *Langmuir*, **34**(13), pp. 3806–3812.
- [7] Chen, J. Z., Troian, S. M., Darhuber, A. A., and Wagner, S., 2005, "Effect of Contact Angle Hysteresis on Thermocapillary Droplet Actuation," *J. Appl. Phys.*, **97**(1), p. 014906.
- [8] Dai, Q., Huang, W., and Wang, X., 2018, "Contact Angle Hysteresis Effect on the Thermocapillary Migration of Liquid Droplets," *J. Colloid Interface Sci.*, **515**, pp. 32–38.
- [9] Kannel, J. W., and Dufrane, K. F., 1986, "Rolling Element Bearings in Space," 20th Aerospace Mechanisms Symposium, Cleveland, OH, May 7–9, pp. 121–132.
- [10] Pratap, V., Moumen, N., and Subramanian, R. S., 2008, "Thermocapillary Motion of a Liquid Drop on a Horizontal Solid Surface," *Langmuir*, **24**(9), pp. 5185–5193.
- [11] Bakli, C., Sree Hari, P. D., and Chakraborty, S., 2017, "Mimicking Wettability Alterations Using Temperature Gradients for Water Nanodroplets," *Nanoscale*, **9**(34), pp. 12509–12515.
- [12] Sathyan, K., Hsu, H. Y., Lee, S. H., and Gopinath, K., 2010, "Long-Term Lubrication of Momentum Wheels Used in Spacecrafts—An Overview," *Tribol. Int.*, **43**(1–2), pp. 259–267.
- [13] Jones, W. R., and Jansen, M. J., 2008, "Tribology for Space Applications," *Proc. Inst. Mech. Eng. Part J J. Eng. Tribol.*, **222**(8), pp. 997–1004.
- [14] Liu, W., Weng, L., and Sun, J., 2009, *Space Lubrication Materials and Technical Manuals*, Science Press, Beijing.
- [15] Roberts, E. W., and Todd, M. J., 1990, "Space and Vacuum Tribology," *Wear*, **136**(1), pp. 157–167.
- [16] Zaretsky, E. V., 1990, "Liquid Lubrication in Space," *Tribol. Int.*, **23**(2), pp. 75–93.
- [17] Chaudhury, M. K., 2003, "Spread the Word About Nanofluids," *Nature*, **423**, pp. 131–132.
- [18] Ke, H., Huang, W., and Wang, X., 2016, "Controlling Lubricant Migration Using Ferrofluids," *Tribol. Int.*, **93**, Part A, pp. 318–323.
- [19] Dai, Q., Li, M., Khonsari, M. M., Huang, W., and Wang, X., 2018, "The Thermocapillary Migration on Rough Surfaces," *Lubr. Sci.*
- [20] Dai, Q., Huang, W., and Wang, X., 2015, "A Surface Texture Design to Obstruct the Liquid Migration Induced by Omnidirectional Thermal Gradients," *Langmuir*, **31**(37), pp. 10154–10160.
- [21] Tian, D., He, L., Zhang, N., Zheng, X., Dou, Y., Zhang, X., Guo, Z., and Jiang, L., 2016, "Electric Field and Gradient Microstructure for Cooperative Driving of Directional Motion of Underwater Oil Droplets," *Adv. Funct. Mater.*, **26**(44), pp. 7986–7992.
- [22] Zhang, M., Wang, L., Hou, Y., Shi, W., Feng, S., and Zheng, Y., 2015, "Controlled Smart Anisotropic Unidirectional Spreading of Droplet on a Fibrous Surface," *Adv. Mater.*, **27**(34), pp. 5057–5062.
- [23] Fusaro, R. L., 2001, "Preventing Spacecraft Failures Due to Tribological Problems," NASA/TM-2001-210806.
- [24] Bonn, D., Eggers, J., Indekeu, J., Meunier, J., and Rolley, E., 2009, "Wetting and Spreading," *Rev. Mod. Phys.*, **81**(2), pp. 739–805.
- [25] Muratore, C., and Voevodin, A. A., 2009, "Chameleon Coatings: Adaptive Surfaces to Reduce Friction and Wear in Extreme Environments," *Annu. Rev. Mater. Res.*, **39**(1), pp. 297–324.
- [26] Öztürk, A., Ezirmik, K. V., Kazmanlı, K., Ürgen, M., Eryılmaz, O. L., and Erdemir, A., 2008, "Comparative Tribological Behaviors of TiN, CrN and MoNc Nanocomposite Coatings," *Tribol. Int.*, **41**(1), pp. 49–59.
- [27] Miyoshi, K., 2007, "Solid Lubricants and Coatings for Extreme Environments: State-of-the-Art Survey," NASA/TM-2007-214668.
- [28] Brochard, F., 1989, "Motions of Droplets on Solid Surfaces Induced by Chemical or Thermal Gradients," *Langmuir*, **5**(2), pp. 432–438.
- [29] Ford, M. L., and Nadim, A., 1994, "Thermocapillary Migration of an Attached Drop on a Solid Surface," *Phys. Fluids*, **6**(9), pp. 3183–3185.
- [30] Dai, Q., Khonsari, M. M., Shen, C., Huang, W., and Wang, X., 2016, "Thermocapillary Migration of Liquid Droplets Induced by a Unidirectional Thermal Gradient," *Langmuir*, **32**(30), pp. 7485–7492.
- [31] Cheng, T., Zhao, B., Chao, J., Meeks, S. W., and Velidandea, V., 2000, "The Lubricant Migration Rate on the Hard Disk Surface," *Tribol. Lett.*, **9**(3–4), pp. 181–185.
- [32] Foroutan, M., Fatemi, S. M., Esmailian, F., Naeni, V. F., and Baniassadi, M., 2018, "Contact Angle Hysteresis and Motion Behaviors of a Water Nano-Droplet on Suspended Graphene Under Temperature Gradient," *Phys. Fluids*, **30**(5), p. 052101.
- [33] Karapetsas, G., Sahu, K. C., and Matar, O. K., 2013, "Effect of Contact Line Dynamics on the Thermocapillary Motion of a Droplet on an Inclined Plate," *Langmuir*, **29**(28), pp. 8892–8906.
- [34] Dussan V, E. B., 1985, "On the Ability of Drops or Bubbles to Stick to Non-Horizontal Surfaces of Solids. Part 2. Small Drops or Bubbles Having Contact Angles of Arbitrary Size," *J. Fluid Mech.*, **151**, pp. 1–20.
- [35] Tadmor, R., 2004, "Line Energy and the Relation Between Advancing, Receding, and Young Contact Angles," *Langmuir*, **20**(18), pp. 7659–7664.
- [36] De Gennes, P., 1985, "Wetting: Statics and Dynamics," *Rev. Mod. Phys.*, **57**(3), pp. 827–863.
- [37] Wasan, D. T., Nikolov, A. D., and Brenner, H., 2001, "Droplets Speeding on Surfaces," *Science*, **291**(5504), pp. 605–606.
- [38] Adamson, A. W., and Gast, A. P., 1997, *Physical Chemistry of Surface*, John Wiley & Sons Inc., New York.
- [39] Hayes, R., Warr, G. G., and Atkin, R., 2010, "At the Interface: Solvation and Designing Ionic Liquids," *Phys. Chem. Chem. Phys.*, **12**(8), pp. 1709–1723.
- [40] Mezger, M., Schröder, H., Reichert, H., Schramm, S., Okasinski, J. S., Schöder, S., Honkikäki, V., Deutsch, M., Ocko, B. M., Ralston, J., Rohwerder, M., Stratmann, M., and Dosch, H., 2008, "Molecular Layering of Fluorinated Ionic Liquids at a Charged Sapphire (0001) Surface," *Science*, **322**(5900), pp. 424–428.